LETTERS
PUBLISHED ONLINE: 4 JANUARY 2016 | DOI: 10.1038/NGEO2630
nature geoscience

Amplification of El Niño by cloud longwave coupling to atmospheric circulation

Gaby Rädel[1], Thorsten Mauritsen[1]*, Bjorn Stevens[1], Dietmar Dommenget[2], Daniela Matei[1], Katinka Bellomo[3] and Amy Clement[4]

The El Niño/Southern Oscillation (ENSO) is the dominant mode of inter-annual variability, with major impacts on social and ecological systems through its influence on extreme weather, droughts and floods[1–3]. The ability to forecast El Niño, as well as anticipate how it may change with warming, requires an understanding of the underlying physical mechanisms that drive it. Among these, the role of atmospheric processes remains poorly understood[4–11]. Here we present numerical experiments with an Earth system model, with and without coupling of cloud radiative effects to the circulation, suggesting that clouds enhance ENSO variability by a factor of two or more. Clouds induce heating in the mid and upper troposphere associated with enhanced high-level cloudiness[12] over the El Niño region, and low-level clouds cool the lower troposphere in the surrounding regions[13]. Together, these effects enhance the coupling of the atmospheric circulation to El Niño surface temperature anomalies, and thus strengthen the positive Bjerknes feedback mechanism[14] between west Pacific zonal wind stress and sea surface temperature gradients. Behaviour consistent with the proposed mechanism is robustly represented in other global climate models and in satellite observations. The mechanism suggests that the response of ENSO amplitude to climate change will in part be determined by a balance between increasing cloud longwave feedback and a possible reduction in the area covered by upper-level clouds.

Warm (El Niño) phases of the El Niño/Southern Oscillation (ENSO) recur on a timescale of typically three to seven years and are characterized by a weaker sea surface temperature (SST) gradient between the Western Pacific warm-pool region and the eastern equatorial Pacific cold tongue region. El Niño is amplified by the positive Bjerknes feedback[14–16] mechanism (Fig. 1a): (1) Positive SST anomalies in the central or eastern Pacific cause (2) local diabatic heating within precipitating deep convective clouds, leading to (3) a weaker Walker circulation and (4) weakened easterlies in the western Pacific, which in turn (5) lessens the tilt of the thermocline and suppresses upwelling of cold deep ocean waters in the east—ultimately leading to further warming of the SSTs. An El Niño event is eventually terminated by ocean Ekman pumping of the warm surface waters away from the equator and by negative atmospheric surface flux feedbacks cooling the upper ocean to restore the climatological east-to-west surface temperature gradient. Thus, El Niño is a complex phenomenon and is influenced by multiple processes. The relative importance of oceanic, atmospheric or coupling processes in shaping the characteristics of ENSO continues to be a matter of scientific debate, with the role of atmospheric feedbacks increasingly emphasized in the recent literature[4–11]. In particular, cloud radiative feedbacks on the surface energy budget are well appreciated[5,7–9], but cloud radiative effects on atmospheric circulation, a topic that has emerged as key to a number of other scientific problems[12,13,17], have not been systematically investigated.

Equatorial Pacific ocean surface temperature anomalies can couple to the atmospheric Walker circulation through various pathways. A direct thermally driven atmospheric circulation response mostly confined to the equator due to rotation[18], thus projecting on the Walker circulation, is excited by enhanced turbulent sensible heat flux from an SST anomaly and latent heat released in precipitating deep convective clouds that tend to occur over the warmest surface waters[19]. Specific patterns of radiative heating and cooling of the tropical atmosphere also act to enhance the ocean–atmosphere coupling as clouds and humidity interact with the circulation in a positive feedback loop to organize the atmosphere into clear regions of subsiding motion and cloudy regions of rising motion[20] (Fig. 1a): upper-level clouds form in humid convectively active regions, reducing the atmospheric radiative cooling of the column, locally heating the middle and upper atmosphere, which induces low-level convergence and rising motion[12]. In regions where the bulk of the atmosphere is dry, the presence of low-level clouds topping the marine boundary layer shifts longwave radiative cooling from the surface to the atmosphere[13]. This cooling of the atmosphere causes low-level divergence and sinking motion, which further dries the free atmosphere above by subsidence, enhancing the contrast between the marine boundary layer and the free atmosphere, leading to more efficient atmospheric cooling. Evidence for such a positive longwave feedback can be observed from space[21], as warm surface temperature anomalies are closely correlated with reductions in outgoing longwave irradiance (Fig. 1b), and thus local radiative heating anomalies of the middle and upper troposphere, as to be expected from enhanced upper-level cloudiness at the outflows of precipitating deep convective clouds.

To elucidate the role of clouds in El Niño we perform and analyse experiments with a state-of-the-art Earth system model, MPI-ESM-LR (ref. 22), with and without cloud radiative processes coupled to the circulation (Methods). The simulation without cloud-circulation interactions is referred to as the experiment with non-interactive clouds, whereas the simulation in which clouds and circulation are allowed to interact is the control experiment. With non-interactive clouds, the surface temperature variance is substantially reduced on inter-annual to decadal timescales

[1]Max Planck Institute for Meteorology, Bundesstrasse 53, 20146 Hamburg, Germany. [2]School of Earth, Atmosphere and Environment, Monash University, 3800 Clayton, Australia. [3]Lamont-Doherty Earth Observatory of Columbia University, 61 Route 9W, Palisades, New York 10964, USA. [4]Rosenstiel School of Marine and Atmospheric Science, University of Miami, 4600 Rickenbacker Causeway, Miami, Florida 33149, USA.
*e-mail: thorsten.mauritsen@mpimet.mpg.de

© 2016 Macmillan Publishers Limited. All rights reserved

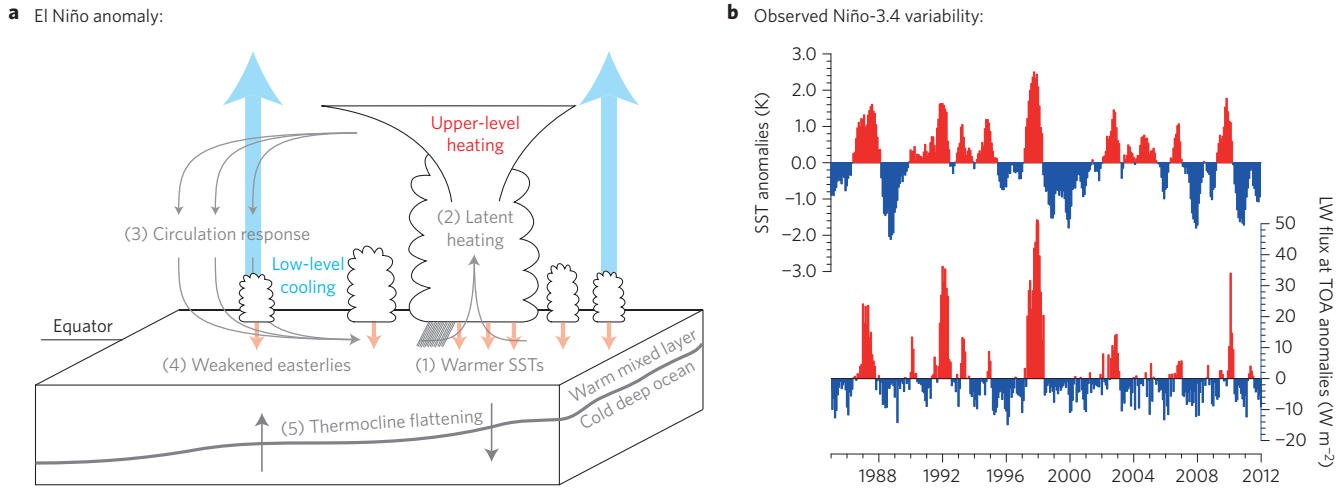

Figure 1 | El Niño circulation anomalies and longwave radiation are closely tied. a, Illustration of the Bjerknes feedback[14] marked as points (1)–(5), showing how clouds influence the strength by longwave heating of the convective regions and cooling of the lower troposphere. **b**, Observed evolution of surface temperature in the Niño-3.4 region according to HadISST (ref. 29) and net longwave (LW) radiation (positive down) reconstructed from various satellite data sets[30].

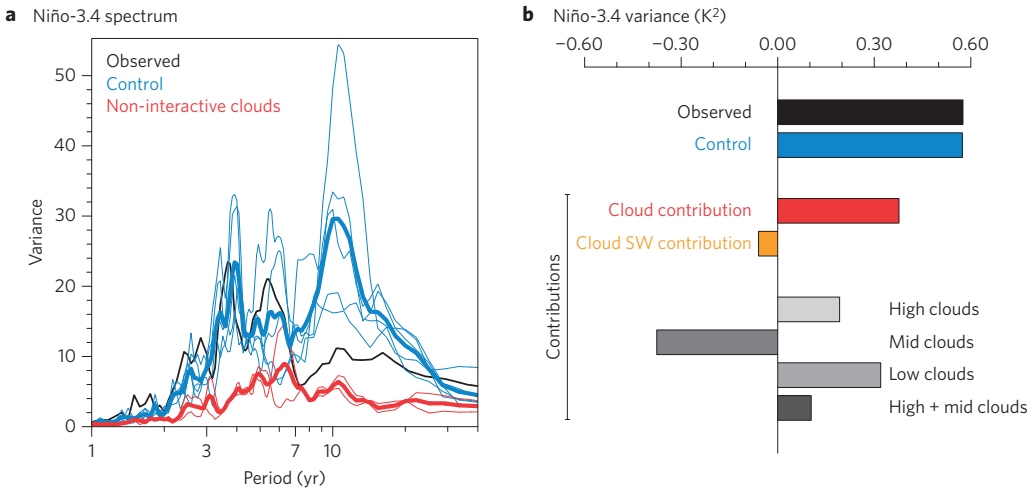

Figure 2 | Impact of cloud-circulation interactions in MPI-ESM-LR on Niño-3.4 variance. a, Normalized variance spectra for HadISST (ref. 29) observations for 1870–2014 (black), the control run (blue) and the two non-interactive clouds runs (red). For the model, thin lines are individual 200-year periods and thick lines are the average. A seven-month filter is applied before calculating the spectra. **b**, Unfiltered Niño-3.4 surface temperature variance in observations and the model. Here contributions to variance are calculated as the difference between control and the respective non-interactive clouds experiment—for example, the red bar is the variance in the control minus that in non-interactive clouds runs. Variances of individual experiments are found in Supplementary Table 1. SW, shortwave.

(Fig. 2a). The control experiment in which clouds are allowed to interact naturally with radiation has three times as great a surface temperature variance as the case with non-interactive clouds. At decadal timescales the model seems to overestimate variability relative to observations, although at these timescales the statistical uncertainty is larger. Total Niño-3.4 variance (Supplementary Table 1) is dominated by the 3–7-year timescales, and the variance in the control matches the observed 1870–2014 variance (0.57 ± 0.04 versus 0.58 ± 0.09 K^2), whereas in the experiment with non-interactive clouds the variance is a factor of three smaller (0.20 ± 0.08 K^2). Variance is additive for statistically independent processes, and thus the experiments show that substantially more than half the Niño-3.4 variance is contributed by cloud feedbacks in MPI-ESM-LR (Fig. 2b) as calculated from the difference between the control and non-interactive clouds experiments. Standard errors are estimated using Monte Carlo methods on a large ensemble of experiments (Methods).

The strong amplification of ENSO variability is entirely due to longwave cloud feedbacks; an additional experiment with only non-interactive clouds in the shortwave exhibits a slight increase in variance of 0.06 ± 0.08 K^2 (Supplementary Table 1), that is, shortwave cloud feedbacks act to dampen variability in MPI-ESM-LR by an equal amount (Fig. 2b). Further experiments wherein clouds are non-interactive only at low, mid and high levels show that most of the amplification in the model is principally carried by the low- and high-level clouds, whereas mid-level clouds alone act to dampen variability. This interpretation is complicated by the fact that clouds correlate in the vertical, so that disabling clouds at one level can amplify or dampen the effect of clouds at other levels. This type of effect is apparent, as the contribution from mid- and high-level clouds is more than the sum of their individual parts (Fig. 2b).

Cloud radiative heating anomalies associated with El Niño act to warm almost the entire tropical atmosphere, peaking at more than 0.2 K per kelvin surface warming at 8–10 km height over the

© 2016 Macmillan Publishers Limited. All rights reserved

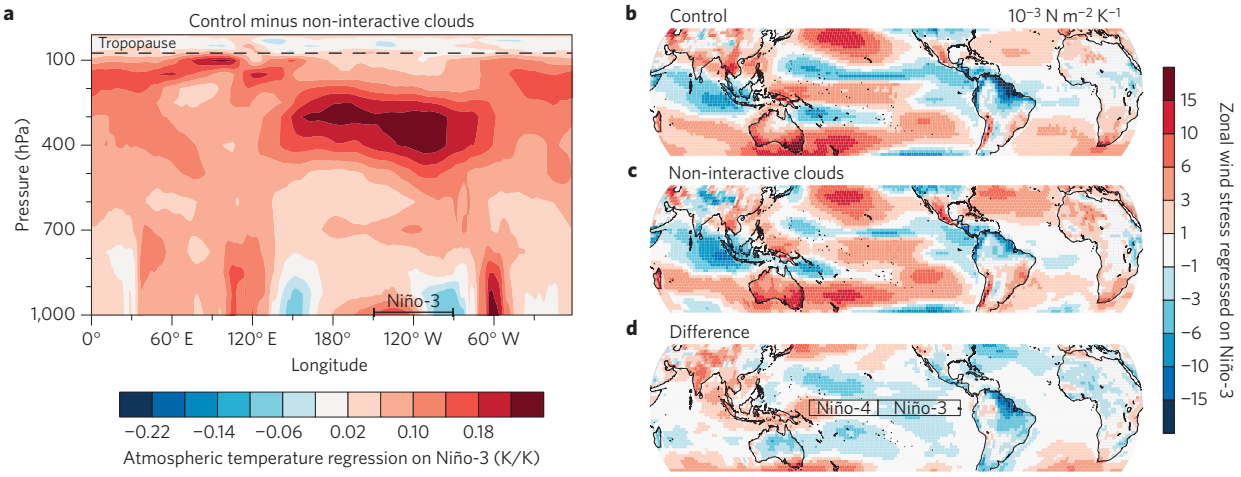

Figure 3 | Cloud radiative heating and cooling patterns enhance the coupling of El Niño to atmospheric circulation. a, Impact of cloud radiative effects on the vertical structure of the temperature response, averaged from 5° S to 5° N, to Niño-3 variability, calculated as the difference between the control and non-interactive clouds experiment in the regression of atmospheric temperature to Niño-3 SST. **b**–**d**, Zonal surface wind stress regressed on Niño-3 SST for the control (**b**) and non-interactive experiments (**c**), and the difference of control minus the non-interactive clouds experiment (**d**).

central Pacific, and to cool at levels below 2 km in the western- and easternmost Pacific in the control experiment relative to the experiment with non-interactive clouds (Fig. 3a). These specific patterns of heating and cooling of the atmosphere by cloud radiative feedbacks strengthen the circulation response at the heart of the Bjerknes feedback: anomalous heating at middle and upper levels leads to local rising motion over the central Pacific, and cooling at low levels in the neighbouring dry zones supports a compensating sinking motion (Fig. 1a). To assess the strength of these effects we measure the Bjerknes feedback strength as the regression of zonal surface wind stress in the western Pacific (Niño-4) to surface temperature in the eastern Pacific (Niño-3), finding that the experiments with non-interactive clouds have reduced feedback strength ($3.9 \pm 0.2 \times 10^{-3}$ versus $3.0 \pm 0.4 \times 10^{-3}$ N m^{-2} K^{-1}). Here it should be noted that the model underestimates the strength of the Bjerknes feedback relative to observations—a feature we shall return to below. Over the warm-pool region in the western Pacific the effect is even more pronounced, where local feedback is reduced to values around 1.0×10^{-3} N m^{-2} K^{-1} in the run with non-interactive clouds (Fig. 3b–d), thereby essentially decoupling the warmest surface waters of the Pacific from contributing to El Niño warming: the prevailing easterlies in the west Pacific are hardly weakened during an El Niño event. Thus, these model experiments suggest that the coupling between longwave atmospheric cloud radiative effects and the circulation plays an important role in determining the modelled Bjerknes feedback strength.

Models are biased in their representation of feedbacks on ENSO. Comprehensive Earth system models systematically underestimate the magnitudes of both the positive Bjerknes feedback and of the negative shortwave cloud feedback[9]. This means that an ability to represent the observed ENSO variance relies on some compensation of errors. Here MPI-ESM-LR is a good example, as despite an excellent reproduction of the observed variance it is one of the models with the weakest Bjerknes feedbacks—which is, however, offset by locally positive shortwave cloud feedback in the easternmost Pacific associated with low-level cloud reductions with surface warming. In observations, the eastern Pacific low-level cloud feedback on surface temperature anomalies is nonlinear, with negative feedback for warm SST anomalies and positive feedback for cold SST anomalies[7]. Together, these model biases would imply that the effect of longwave cloud feedbacks in the real world are even larger than those found in the present study; a hypothesis that could be tested by repeating the experiment with a more realistic model.

An observed positive relationship between anomalous net top of atmosphere (TOA) longwave irradiance and Niño-3.4 SST anomalies is robustly represented across available CMIP5 models, and there also is a striking similarity in spatial structure, with heating in the central Pacific and cooling in neighbouring regions (Fig. 4b–d and Supplementary Figs 4–7 and Supplementary Table 4). In the experiment with non-interactive clouds the pattern strength is greatly reduced (Fig. 4e). The residual positive feedback in the western Pacific in the run with non-interactive clouds is presumably associated with water vapour feedbacks. All of the CMIP5 models that were available for analysis exhibit a spatial maximum longwave feedback (Methods) that exceeds this background by a factor two or more (Fig. 4a). Together, this suggests that the coupling of cloud longwave radiative effects on the circulation enhances the Bjerknes feedback both in other models, as well as in the real world, relative to the case of non-interactive clouds. Noteworthy is that models in general, and MPI-ESM-LR in particular, have the peak positive longwave feedback further west than is observed and that they underestimate the longwave cooling over the Maritime Continent. This could help explain the overly weak Bjerknes feedback in models[9], as it is the contrast between heating and cooling that will determine the strength of the circulation response. The presented analysis tells only half the story, as the surface flux is needed to investigate the full cloud longwave effect on the atmospheric circulation, and long-term measurements of the surface radiation budget across the Pacific would make it possible to test these ideas.

An understanding of the role of cloud radiative effects in modulating the Bjerknes feedback loop could guide future model improvements that ultimately improve the representation of El Niño in ways that go beyond the common error compensation between under-represented positive and negative feedbacks[9]. For example, in the past we found that increasing the rate of conversion from cloud water to precipitation in MPI-ESM leads to a weaker ENSO variability[23]. At the time this response was puzzling, as according to conventional understanding a greater amount of convective heating should strengthen the Bjerknes feedback, and hence ENSO variability. Our present findings suggest an interpretation: because a higher precipitation efficiency also means less condensate is detrained into the environment, upper-level cloudiness is reduced, which instead weakens the cloud longwave heating associated with El Niño. More generally, most models produce too few, but too reflective tropical low-level clouds[24]—probably a result of the need to maintain the global radiation balance in models, despite

© 2016 Macmillan Publishers Limited. All rights reserved

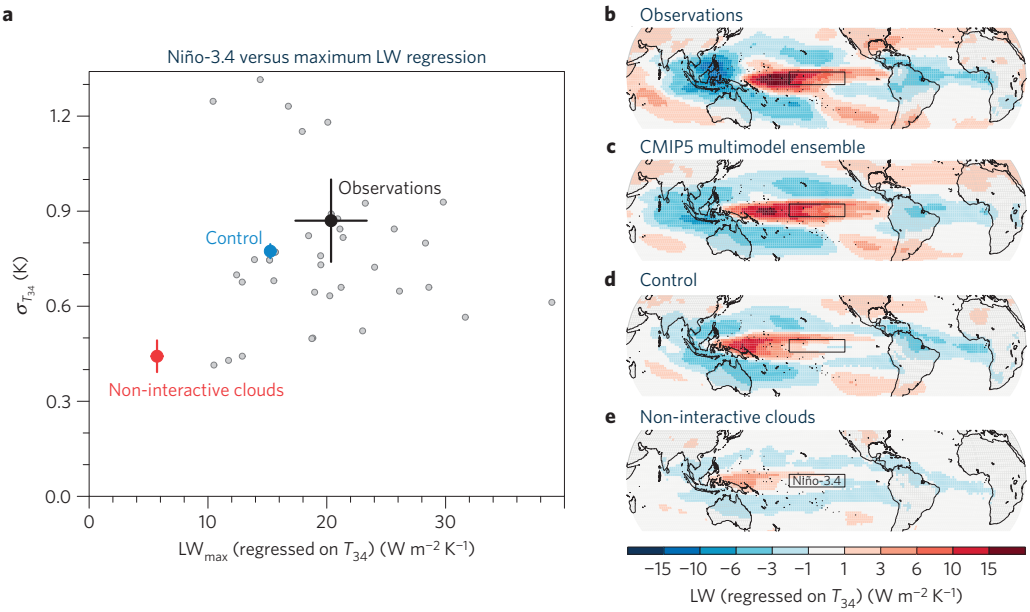

Figure 4 | TOA longwave feedback in observations and in models (Supplementary Table 4). a, Scatter plot of Niño-3.4 standard deviation versus the spatial maximum net longwave flux (positive down) regressed on Niño-3.4 (Methods). Error bars are standard errors on the mean calculated using a Monte Carlo approach as described in Methods. **b**–**e**, Maps of regressions: observations (**b**); CMIP5 multimodel ensemble (**c**); control (**d**); non-unteractive clouds (**e**). Observations of SST (ref. 29) and TOA radiation[30] are for the period 1985–2012. In this analysis, except for observations, surface air temperature from models was used because not all CMIP5 models provided surface temperature.

deficient representations of boundary-layer processes—however, for the identified atmospheric low-level longwave cooling it is primarily the cloud cover, not the optical thickness, that controls atmospheric emissivity. Thus, greater fidelity in modelled low-level cloudiness could improve the representation of ENSO-related feedbacks. Finally, we believe that improving models' ability to aggregate convection into large precipitating cloud clusters and suppress convection in the surroundings would strengthen the contrast between radiative cooling and heating, and augment the coupling to the atmospheric circulation.

The radiative coupling between clouds, circulation and the Bjerknes feedback proposed here is complementary to past diagnostic studies that aimed at separating dynamic and surface flux feedbacks[5,8,9]. Our results also enrich the theoretical framework for understanding possible impacts of a changing climate on El Niño. Past model-based studies have found no consensus concerning changes in frequency nor amplitude, but suggest that extreme El Niño events become more frequent in a warming climate[25], whereas evidence from the early Pliocene, when temperatures were higher than today, suggest relatively calm conditions in the Pacific, with characteristic permanent El Niño conditions[26]. In a warming climate the cloud longwave feedback on ENSO can be expected to increase because the contrast in outgoing longwave radiation between clear and cloudy regions increases; an effect of upper-level clouds rising to maintain an approximately fixed temperature[27]. However, if, as has been suggested, the areal coverage of upper-level clouds might decrease in a warming climate[28], this would act to weaken ENSO. This way, a fundamental understanding of tropical convective cloud feedbacks could eventually strengthen confidence in how ENSO responds to warming.

Methods

Methods and any associated references are available in the online version of the paper.

Received 8 July 2015; accepted 2 December 2015;
published online 4 January 2016

References

1. Nicholls, N., Lavery, B., Frederiksen, C., Drosdowsky, W. & Torok, S. Recent apparent changes in relationships between the El Niño–Southern Oscillation and Australian rainfall and temperature. *Geophys. Res. Lett.* **23,** 3357–3360 (1996).
2. Dai, A., Trenberth, K. E. & Karl, T. R. Global variations in droughts and wet spells: 1990–1995. *Geophys. Res. Lett.* **25,** 3367–3370 (1998).
3. Barnard, P. L. *et al.* Coastal vulnerability across the Pacific dominated by El Niño/Southern Oscillation. *Nature Geosci.* **8,** 801–807 (2015).
4. Guilyardi, E. *et al.* Representing El Niño in coupled ocean-atmosphere GCMs: the dominant role of the atmosphere component. *J. Clim.* **17,** 4623–4629 (2004).
5. Sun, D. Z. *et al.* Radiative and dynamical feedbacks over the equatorial cold tongue: results from nine atmospheric GCMs. *J. Clim.* **19,** 4059–4074 (2006).
6. Dommenget, D. The slab ocean El Niño. *Geophys. Res. Lett.* **37,** L20701 (2010).
7. Lloyd, J., Guilyardi, E. & Weller, H. The role of atmospheric feedbacks during ENSO in CMIP3 models. Part III: the shortwave flux feedback. *J. Clim.* **25,** 4275–4293 (2012).
8. Chen, L., Yu, Y. & Sun, D.-Z. Cloud and water vapor feedbacks to the El Niño warming: are they still biased in CMIP5 models? *J. Clim.* **26,** 4947–4961 (2013).
9. Bellenger, H., Guilyardi, E., Leloup, J., Lengaigne, M. & Vialard, J. ENSO representation in climate models: from CMIP3 to CMIP5. *Clim. Dynam.* **42,** 1999–2018 (2014).
10. Chen, D. *et al.* Strong influence of westerly wind bursts on El Niño diversity. *Nature Geosci.* **8,** 339–345 (2015).
11. Chen, X. & Wallace, J. M. ENSO-like variability: 1900–2013. *J. Clim.* http://dx.doi.org/10.1175/JCLI-D-15-0322.1 (2015).
12. Bretherton, C. S. & Sobel, A. H. A simple model of a convectively coupled Walker circulation using the weak temperature gradient approximation. *J. Clim.* **15,** 2907–2920 (2002).
13. Muller, C. J. & Held, I. M. Detailed investigation of the self-aggregation of convection in cloud-resolving simulations. *J. Atmos. Sci.* **69,** 2551–2565 (2012).
14. Bjerknes, J. Atmospheric teleconnections from the equatorial Pacific. *Mon. Weath. Rev.* **97,** 163–172 (1969).
15. Wyrtki, K. El Niño—the dynamic response of the equatorial Pacific Ocean to atmospheric forcing. *J. Phys. Oceanogr.* **5,** 572–584 (1975).
16. Cane, M. & Zebiak, S. A theory for El Niño and the Southern Oscillation. *Science* **228,** 1085–1087 (1985).
17. Bony, S. *et al.* Clouds, circulation and climate sensitivity. *Nature Geosci.* **8,** 261–268 (2015).
18. Gill, A. E. Some simple solutions for heat-induced tropical circulation. *Q. J. R. Meteorol. Soc.* **106,** 447–462 (1980).
19. Emanuel, K. A., Neelin, J. D. & Bretherton, C. S. On large-scale circulation in convecting atmospheres. *Q. J. R. Meteorol. Soc.* **120,** 1111–1143 (1994).

© 2016 Macmillan Publishers Limited. All rights reserved

20. Nilsson, J. & Emanuel, K. A. Equilibrium atmospheres of a two-column radiative-convective model. *Q. J. R. Meteorol. Soc.* **125,** 2239–2264 (1999).
21. Chiodi, A. & Harrison, D. Characterizing warm-ENSO variability in the equatorial Pacific: an OLR perspective. *J. Clim.* **23,** 2428–2439 (2010).
22. Giorgetta, M. *et al.* Climate and carbon cycle changes demo 1850 to 2100 in MPI-ESM simulations for the Coupled Model Intercomparison Project phase 5. *J. Adv. Model. Earth Syst.* **5,** 572–597 (2013).
23. Mauritsen, T. *et al.* Tuning the climate of a global model. *J. Adv. Model. Earth Syst.* **4,** M00A01 (2012).
24. Nam, C., Bony, S., Dufresne, J.-L. & Chepfer, H. The 'too few, too bright' tropical low-cloud problem in CMIP5 models. *Geophys. Res. Lett.* **39,** L21801 (2012).
25. Cai, W. *et al.* Increasing frequency of extreme El Niño events due to greenhouse warming. *Nature Clim. Change* **4,** 111–116 (2014).
26. Fedorov, A. V. *et al.* The pliocene paradox (mechanisms for a permanent El Niño). *Science* **312,** 1485–1489 (2006).
27. Hartmann, D. & Larson, K. An important constraint on tropical cloud-climate feedback. *Geophys. Res. Lett.* **29,** 1951 (2002).
28. Mauritsen, T. & Stevens, B. Missing iris effect as a possible cause of muted hydrological change and high climate sensitivity in models. *Nature Geosci.* **8,** 346–351 (2015).
29. Rayner, N. A. *et al.* Global analyses of sea surface temperature, sea ice, and night marine air temperature since the late nineteenth century. *J. Geophys. Res.* **108,** 4407 (2003).
30. Allan, R. P. *et al.* Changes in global net radiative imbalance 1985–2012. *Geophys. Res. Lett.* **41,** 5588–5597 (2014).

Acknowledgements

This work is supported by the Max-Planck-Gesellschaft (MPG) and funding by the Federal Ministry for Education and Research in Germany (BMBF) through the research programme MiKlip project FKZ:01LP1128B. Computational resources were made available by Deutsches Klimarechenzentrum (DKRZ) through support from BMBF and by the Swiss National Supercomputing Centre (CSCS). D.D. acknowledges support from the ARC Centre of Excellence for Climate System Science grant CE110001028 and project DP120101442. D.M. acknowledges support from BMBF through the cooperative Project RACE.

Author contributions

B.S., G.R. and T.M. conceived the original idea for this study. G.R. and T.M. developed the methodology and conducted the experiments. The bulk of the analysis was done by G.R., T.M., B.S. and D.M., although all authors contributed to the interpretation of the results. G.R. and T.M. led the writing of the manuscript with contributions and input from all authors.

Additional information

Supplementary information is available in the online version of the paper. Reprints and permissions information is available online at www.nature.com/reprints. Correspondence and requests for materials should be addressed to T.M.

Competing financial interests

The authors declare no competing financial interests.

© 2016 Macmillan Publishers Limited. All rights reserved

Methods

We study the impact of cloud feedbacks on ENSO variability by comparing a standard pre-industrial control simulation with a global climate model—comprising atmosphere, land and ocean—to a simulation with the same model set-up wherein cloud feedbacks are disabled. We use a modified version of the Max Planck Institute (MPI) for Meteorology Earth System Model at low resolution (MPI-ESM-LR; ref. 22), which corresponds to T63 horizontal resolution and 47 vertical levels in the atmosphere with a nominal 1.5° horizontal resolution and 40 vertical levels in the ocean component, as was used in the fifth phase of the Coupled Model Intercomparison Project CMIP5 (ref. 31).

The method of disabling feedbacks has been developed for ECHAM6 (ref. 32). It consists of two steps: first, a standard simulation with fully interactive cloud feedbacks is performed where all relevant instantaneous fields—that is, cloud fraction, cloud liquid water content, cloud ice water content and cloud droplet number concentration—are written out at every 2-hourly radiation call. Second, in a simulation with an identical set-up these fields are read into the model's radiation calculations at every radiation call at the same time of day and year. Here we stored model data for 50 years from the first simulation, and subsequently ran the model for 250 years. In contrast to ref. 32, which presented the radiation code with stored clouds in the sequence they appeared in the control simulation, the fields are here selected randomly from one of the 50 previously simulated years, thereby eliminating auto-correlation in the imposed cloud fields. This change with respect to the original method eliminates possible imposed low-frequency variability resulting from clouds because scenes that auto-correlate in time could imprint on the variability. Two realizations were made with all clouds non-interactive, whereby clouds were read into the model in different orders to perturb the evolution of the model. Further, an experiment with only non-interactive clouds in the shortwave part of the radiation code, and experiments with only non-interactive clouds at low level (below 700 hPa), mid level (400–700 hPa), high level (above 400 hPa) and combined mid and high levels (above 700 hPa) were conducted.

The procedure leads to a weak warming drift (Supplementary Fig. 1) in the experiment with non-interactive clouds, which becomes acceptable for the purpose of this study after a few decades of the 250-year run. Therefore, the first 50 years of the simulations have not been considered, whereafter the linear trend has been removed in the presented analysis. Slightly larger warming drifts are found when mid- and high-level clouds are non-interactive, and a cooling drift is found when low-level clouds are non-interactive. For comparison, the span between different CMIP5 models is about 3 K (ref. 23)—that is, the absolute global mean temperature in all the simulations presented are within the CMIP5 ensemble. Perhaps more importantly for the present study, there is no substantial change in the spatial structure of surface temperature in the tropical Pacific (Supplementary Fig. 2). In particular, the mean state zonal gradient across the basin is practically unchanged.

We calculate surface temperature variance on the widely used Niño-4, Niño-3.4 and Niño-3 regions (marked in Figs 3 and 4) and, for completeness, the Niño-1+2 region near the coast of Ecuador and Peru (Supplementary Table 1). The overall conclusions of this study are independent of the choice of region, except for Niño-1+2. Classical Bjerknes (μ) and surface flux feedbacks (α) are tabulated for the experiments in Supplementary Table 2. Here μ is calculated as the regression of Niño-4 zonal surface wind stress on Niño-3 SST, and the surface flux feedback is the regression of the net flux of shortwave, longwave, latent and sensible heat fluxes averaged over Niño-3 against SST in the same region.

Estimating uncertainty in El Niño-related measures is challenging because the signals are modulated on timescales of the order of and longer than the observed record. Here we make use of a 100-member ensemble of historical simulations conducted with MPI-ESM1.1-LR, the successor to MPI-ESM-LR, which is used elsewhere in this study. The runs are started from different initial conditions taken from a long control simulation. Each member provides one estimate of a measure, say $\sigma_{T3.4}$ as demonstrated in Supplementary Fig. 3, and from the resulting distribution the standard error on the respective measure can be calculated. These are, however, relevant only for averages over 155-year periods. Therefore, to provide standard error estimates on the various record lengths used in this study we rescale the standard error using the square root of the ratio to the actual record length (Supplementary Table 3). For the uncertainty of the maximum longwave regression in the observed record we use the Niño-4 longwave regression standard error scaled up by the mean regression to $\pm 3\ \mathrm{W\,m^{-2}\,K^{-1}}$, because MPI-ESM1.1-LR is biased low with respect to this regression. Elsewhere we apply the standard error estimate from the large ensemble.

For the analysis of CMIP5 (ref. 31) model results presented in Fig. 4 we used all models available to us, which provided the variables needed for the analysis (refs 33–53, Supplementary Table 4). Because models place their longwave response to Niño-3.4 SST anomalies in slightly varying positions (Supplementary Figs 4–7) we present the spatial maximum of the net longwave flux regression in Fig. 4.

Data sources. HadISST data are provided by the UK Met Office Hadley Centre (http://www.metoffice.gov.uk/hadobs/hadisst), TOA irradiance fluxes are provided by R. Allan (http://www.met.reading.ac.uk/~sgs02rpa/research/DEEP-C/GRL), and CMIP5 data from the coupled modelling groups (Supplementary Table 4) coordinated by the World Climate Research Programme's Working Group on Coupled Modelling (http://cmip-pcmdi.llnl.gov/cmip5).

Code availability. The MPI-ESM model is available on http://www.mpimet.mpg.de/en/science/models/mpi-esm.html. Code changes used in this study are in the software repository revision 8061. Code and scripts used in the analysis and other supplementary information are archived by the Max Planck Institute for Meteorology and can be obtained by either contacting the corresponding author or from publications@mpimet.mpg.de.

References

31. Taylor, K. E., Stouffer, R. J. & Meehl, G. A. An overview of CMIP5 and the experiment design. *Bull. Am. Meteorol. Soc.* **93,** 485–498 (2012).
32. Mauritsen, T. *et al.* Climate feedback efficiency and synergy. *Clim. Dynam.* **41,** 2539–2554 (2013).
33. Bi, D. *et al.* The ACCESS coupled model: description, control climate and evaluation. *Aust. Meteorol. Oceanogr. J.* **63,** 41–64 (2013).
34. Xiao-Ge, X. *et al.* How well does BCC CSM1.1 reproduce the 20th century climate change over China? *Atmos. Ocean. Sci. Lett.* **6,** 21–26 (2012).
35. Ji, D. *et al.* Description and basic evaluation of BNU-ESM version 1. *Geosci. Model Dev.* **7,** 1601–1647 (2014).
36. von Salzen, K. *et al.* The Canadian fourth generation atmospheric global climate model (CanAM4). Part I: representation of physical processes. *Atmos. Ocean* **51,** 104–125 (2013).
37. Meehl, G. A. *et al.* Climate system response to external forcings and climate change projections in CCSM4. *J. Clim.* **25,** 3661–3683 (2012).
38. Meehl, G. A. *et al.* Climate change projections in CESM1(CAM5) compared to CCSM4. *J. Clim.* **26,** 6287–6308 (2013).
39. Voldoire, A. *et al.* The CNRM-CM5.1 global climate model: description and basic evaluation. *Clim. Dynam.* **40,** 2091–2121 (2012).
40. Rotstayn, L. D. *et al.* Aerosol- and greenhouse gas-induced changes in summer rainfall and circulation in the Australasian region: a study using single-forcing climate simulations. *Atmos. Chem. Phys.* **12,** 6377–6404 (2012).
41. Li, L. *et al.* The flexible global ocean-atmosphere-land system model, Grid-point Version 2: FGOALS-g2. *Adv. Atmos. Sci.* **30,** 543–560 (2013).
42. Donner, L. J. *et al.* The dynamical core, physical parameterizations, and basic simulation characteristics of the atmospheric component AM3 of the GFDL global coupled model CM3. *J. Clim.* **24,** 3484–3519 (2011).
43. Dunne, J. P. *et al.* GFDL's ESM2 global coupled climate–carbon earth system models. Part I: physical formulation and baseline simulation characteristics. *J. Clim.* **25,** 6646–6665 (2012).
44. Schmidt, G. A. *et al.* Configuration and assessment of the GISS ModelE2 contributions to the CMIP5 archive. *J. Adv. Model. Earth Syst.* **6,** 141–184 (2014).
45. Jones, C. D. *et al.* The HadGEM2-ES implementation of CMIP5 centennial simulations. *Geosci. Model Dev.* **4,** 543–570 (2011).
46. Volodin, E. M., Dianskii, N. A. & Gusev, A. V. Simulating present-day climate with the INMCM4.0 coupled model of the atmospheric and oceanic general circulations. *Izv. Atmos. Ocean. Phys.* **46,** 414–431 (2010).
47. Dufresne, J. L. *et al.* Climate change projections using the IPSL-CM5 Earth System Model: from CMIP3 to CMIP5. *Clim. Dynam.* **40,** 2123–2165 (2013).
48. Hourdin, F. *et al.* LMDZ5B: the atmospheric component of the IPSL climate model with revisited parameterizations for clouds and convection. *Clim. Dynam.* **40,** 2193–2222 (2013).
49. Watanabe, M. *et al.* Improved climate simulation by MIROC5: mean states, variability, and climate sensitivity. *J. Clim.* **23,** 6312–6335 (2010).
50. Watanabe, S. *et al.* MIROC-ESM 2010: model description and basic results of CMIP5-20c3m experiments. *Geosci. Model Dev.* **4,** 845–872 (2011).
51. Stevens, B. *et al.* Atmospheric component of the MPI-M Earth System Model: ECHAM6. *J. Adv. Model. Earth Syst.* **5,** 146–172 (2013).
52. Yukimoto, S. *et al.* A new global climate model of the meteorological research institute: MRI-CGCM3: model description and basic performance. *J. Meteorol. Soc. Jpn* **90A,** 23–64 (2012).
53. Bentsen, M. *et al.* The Norwegian Earth System Model, NorESM1-M–Part 1: description and basic evaluation of the physical climate. *Geosci. Model Dev.* **6,** 687–720 (2013).

© 2016 Macmillan Publishers Limited. All rights reserved